# An analysis of internal strains in unidirectional and chopped graphite fibre composites based on x-ray diffraction and micro Raman spectroscopy measurements

B. Benedikt, M. Lewis & P. Rangaswamy
*Engineering Sciences and Application Division,*
*Los Alamos National Laboratory, USA*

## Abstract

In this paper, the method for the determination of internal strains in polymer matrix composites from the strain measurements in the embedded sensors has been examined. Two types of strain sensors embedded in either chopped graphite fibre/epoxy matrix composite or unidirectional graphite fibre/polyimide matrix composite were investigated. For the chopped fibre composite, we used Kevlar-49 fibres (~10μm in diameter) as strain sensors, while aluminium inclusions with diameters ranging from 1 to 20μm were embedded in the unidirectional composite. Both composite plates with embedded sensors were subjected to external loads generated by a four-point bending fixture. Strains inside the sensors were measured using either x-ray diffraction (XRD) or micro Raman spectroscopy (MRS). A model based on the equivalent inclusion method (EIM) was used to extract the internal strains in composites from the measured strains inside the embedded sensors. It has been demonstrated that the geometrical features and the material properties of the embedded strain sensors may affect the accuracy of the extraction of the composite internal strains. The average interactions between the sensors were found to have only a minor effect on the strain determination in a composite.
*Keywords: x-ray diffraction; micro Raman spectroscopy; equivalent inclusion method; Eshelby tensor; interactions between inclusions; four-point bending.*

# 1 Introduction

There are several experimental methods presented in the literature that can be used to measure internal strains in polymer matrix composites (Benedikt et al. [1]). Unfortunately, the majority of the proposed experimental approaches can only be used to determine strains averaged over a macroscopic gauge volume (layer removal, hole-drilling, etc.). In this work, we discuss a non-destructive method that can be used to determine strains in polymer matrix composites at microscopic level. The presented method is based on strain measurements in embedded sensors. For the purpose of this work, the strain measurements in the sensors were performed using either x-ray diffraction (XRD) or micro Raman spectroscopy (MRS).

The idea of employing embedded metallic inclusions as XRD strain sensors was first proposed by Predecki and Barrett (Predecki and Barrett [2]) and used to measure internal strains in unidirectional graphite/epoxy composites with embedded aluminium, silver, and niobium inclusions. These authors successfully measured the strains in the inclusions embedded in composite plates subjected to mechanical loads. However, they were unable to quantitatively evaluate the strain transfer from the composites to the embedded inclusions, which is critical for the correct determination of the state of strain in the composites.

The use of MRS to study strain distributions with μm resolution in fibre composites was first reported by Galiotis [3]. It has been shown by this author that the initiation of fibre debonding, matrix yielding, and strain transfer efficiency in short- and long-fibre composites can be assessed by MRS. The possibility to use the reinforcing fibres as MRS strain sensors is another feature of MRS technique. However, MRS is generally less accurate than XRD and it can only be used to measure longitudinal strains in a fibre.

The main objective of the work presented in this paper is to assess the accuracy of the strain determination in polymer matrix composites from the measurements in the embedded sensors. As an illustration, we consider two types of embedded sensors, namely Kevlar-49 fibres embedded in a graphite/epoxy composite and aluminium inclusions embedded in a graphite/polyimide composite. Strain in a Kevlar-49 fibre was measured using MRS, while XRD was employed to measure strains in Al inclusions. Both types of composite samples with embedded sensors were subjected to four-point bending conditions generated by the same fixture. To extract the strain field in a composite from the experimental data the model based on the equivalent inclusion method (EIM) was used. Obviously, the presence of the embedded sensors locally disturbs the strain field; moreover the geometry, elastic properties, interactions between the sensors, and spatial orientation of the sensors also affect the local strain disturbance. Therefore, the numerical model must be able to take all these factors into an account to accurately extract composite strains from the measurements in the embedded sensors. Finally, we want to point out that residual strains in the sensors were not investigated in this paper. However, it has been shown by Benedikt et al. [4] that the residual strains can be quite accurately determined using the present method.

# 2 Fundamental basis of the method

## 2.1 X-ray diffraction

The experimental determination of the strains in Al inclusions embedded in the unidirectional graphite/polyimide composite was done using a Siemens D500 diffractometer fitted with pseudo parallel-beam optics and a solid-state detector. First, the lattice spacing $d_0$ for 422 atomic planes for unstressed Al powder was measured. Second, the lattice spacing $d_{\phi,\psi}$ for 422 planes for the embedded Al inclusions oriented along a direction defined by $\phi$ (in-plane) and $\psi$ (out-of-plane) angles was experimentally obtained as a function of the prescribed bending moment. The direction of the reinforcing fibres coincided with $\phi = 0^0$ direction. The relationships between the measured lattice spacing and the principal components of the strain ($\varepsilon_{11}$, $\varepsilon_{22}$, and $\varepsilon_{33}$) in the inclusions are given by eqn (1-2).

$$\frac{d_{\phi=0,\psi} - d_0}{d_0} = (\varepsilon_{11} - \varepsilon_{33})\sin^2\psi + \varepsilon_{33} \tag{1}$$

$$\frac{d_{\phi=90,\psi} - d_0}{d_0} = (\varepsilon_{22} - \varepsilon_{33})\sin^2\psi + \varepsilon_{33} \tag{2}$$

In the numerical computations, six different values of the lattice spacing $d_{\phi,\psi}$ were measured for each $\phi$ angle ($\phi=0^0$ or $\phi=90^0$) by varying $\psi$. It can be shown that if $\frac{d_{\phi,\psi} - d_0}{d_0}$ vs. $\sin^2\psi$ plots for $\phi=0^0$ and $0^0<\psi< 90^0$, and $\phi=90^0$ and $0°<\psi<90°$ are linear, then the shear stress components $\sigma_{13}$ and $\sigma_{23}$ are zero, there are no significant stress gradients in the diffracting volume, and the method is considered to be applicable to the specimens being measured (Noyan and Cohen [5]).

## 2.2 Micro Raman spectroscopy

Strain measurements using Raman spectroscopy are possible in materials for which the strain field changes the inter-atomic force constants and molecular vibration frequencies. The change of the molecular vibration frequencies affects the measured frequency of the scattered radiation causing a shift of the Raman peak. For Kevlar-49 fibres and many other materials there is a linear relationship between the applied longitudinal strain and the Raman peak shift. In the present study, the Raman peak due to the phenyl ring stretching vibration near 1610 $cm^{-1}$ was chosen to determine the state of strain in Kevlar-49 fibres, since this particular vibration mode exhibits the highest strain sensitivity. The strain dependence of the Kevlar 49 fibre Raman peak position was taken to be 4.13$cm^{-1}$ per % of longitudinal strain. Only fibre longitudinal strains were measured using MRS technique.

For the light source, we used an Innova 70C $Ar^+$ laser that generated a laser beam with 488 nm wavelength. An ACTON SpectraPro® 500i spectrometer

equipped with a CCD chip and a Keiser Optical Systems Inc. Raman microscope were used to record the Raman spectra. A camera attached to the microscope was used to monitor the irradiated area. The spatial resolution of the MRS measurements was about 8μm. The laser power on a sample was kept at less than 0.8 mW to avoid local heating.

### 2.3 Equivalent inclusion method

The objective of the numerical model is to accurately extract the strains in the composites from the measured strains in the embedded sensors. Different assumptions were made to compute composite strains from XRD and MRS data. These assumptions along with the fundamental equations used in the computations are presented in this section.

The Al inclusions used in XRD measurements locally formed clusters with high concentrations of inclusions within a cluster. Therefore, the average distance between the inclusions in the densely packed clusters could be very small with respect to inclusions size. Consequently, the local interactions between the embedded inclusions could considerably disturb the strain field, which could also affect the XRD data. Moreover, the volume irradiated by x-ray beam was much larger than any individual inclusion. Therefore, the XRD strains in the inclusions represent strains averaged over the volume of a cluster. To numerically estimate the inaccuracy of the method caused by the averaged interactions between inclusions, we used the model proposed by Benedikt et al. [6].

It would be very difficult to numerically determine the interactions between all individual Al inclusions in an average size cluster due to the sheer number of inclusions, which could be larger than several thousands. On the other hand, the individual interactions are only considerable between the inclusions, which are located fairly close to each other (Benedikt et al. [6]). For these reasons, we explicitly modelled the interactions only inside a relatively small sub-cluster that consisted of up to no more than 60 inclusions. By prescribing the far-field strains $\boldsymbol{\varepsilon}^{\mathbf{T\text{-}M}}$ to the sub-cluster, the average influence of the remaining inclusions in the cluster was modelled. The magnitude of $\boldsymbol{\varepsilon}^{\mathbf{T\text{-}M}}$ was determined using the following equations:

$$C^{I}_{ijkl}\left(\varepsilon^{Bend}_{kl}+\varepsilon^{d(p)}_{kl}+\varepsilon^{T-M}_{kl}\right)=C^{M}_{ijkl}\left(\varepsilon^{Bend}_{kl}+\varepsilon^{d(p)}_{kl}-\varepsilon^{*(p)}_{kl}+\varepsilon^{T-M}_{kl}\right)\quad \text{p=1,…,N} \tag{3}$$

$$\frac{v_f}{N}\sum_{p=1}^{N}\left(C^{M}_{ijkl}\left(\varepsilon^{Bend}_{kl}+\varepsilon^{d(p)}_{kl}-\varepsilon^{T(p)}_{kl}+\varepsilon^{T-M}_{kl}\right)\right)+(1-v_f)\left(C^{M}_{ijkl}\left(\varepsilon^{Bend}_{kl}+\varepsilon^{T-M}_{kl}\right)\right)=C^{M}_{ijkl}\varepsilon^{Bend}_{kl} \tag{4}$$

$$C^{I}_{ijkl}\varepsilon^{X-Ray}_{kl}=\frac{1}{N}\sum_{p=1}^{N}C^{I}_{ijkl}\left(\varepsilon^{Bend}_{kl}+\varepsilon^{d(p)}_{kl}+\varepsilon^{T-M}_{kl}\right) \tag{5}$$

where $\boldsymbol{\varepsilon}^{\mathbf{X\text{-}Ray}}$ is the measured strain in the inclusions (for MRS experiments $\boldsymbol{\varepsilon}^{\mathbf{X\text{-}Ray}}$ is substituted with $\boldsymbol{\varepsilon}^{\mathbf{MRS}}$ - strain measured in a Kevlar-49 fibre), $\mathbf{C}^{\mathbf{I}}$ is the tensor of the elastic constants of the inclusions, $\mathbf{C}^{\mathbf{M}}$ is tensor of the elastic properties of the matrix, $\boldsymbol{\varepsilon}^{\mathbf{Bend}}$ is the unknown strain in composite caused by external bending, $v_f$ is the average volume fraction of the inclusions, N is the number of inclusions in

the sub-cluster, $\boldsymbol{\varepsilon}^{\mathbf{T(p)}}$ is the constant eigenstrain for the p[th] inclusion and $\boldsymbol{\varepsilon}^{\mathbf{d(p)}}$ is the disturbance strain for the p[th] inclusion given by:

$$\varepsilon_{ij}^{d(I)} = S_{ijkl}^{\Omega(I)} \varepsilon_{kl}^{T(I)} + \sum_{\substack{r=1 \\ (r \neq I)}}^{N} S_{ijkl}^{\Omega(r)(outside)}\Big|_{x=x_p} \varepsilon_{kl}^{T(r)} \quad \text{for I=1, 2,…,N} \tag{6}$$

where $S^{\Omega(I)}$ is the Eshelby tensor for the interior points of I[th] spherical inclusion, and $S^{\Omega(r)(outside)}$ is the Eshelby tensor for the exterior points of r[th] spherical inclusion computed at the centre point $\mathbf{x_p}$ of r[th] inclusion (Eshelby [7]). Since the numerical values of the Eshelby tensors for the exterior points depend on the relative position of the interacting inclusions, the disturbance strains $\boldsymbol{\varepsilon}^{\mathbf{d(p)}}$ (p=1, 2,…,N) include the effect of individual interactions. From the solution of eqn (3-6) the unknown $\boldsymbol{\varepsilon}^{\mathbf{Bend}}$ strain can be also computed. $\boldsymbol{\varepsilon}^{\mathbf{Bend}}$ is assumed to be identical to the strain in the composite generated by external bending at locations occupied by the embedded sensors.

For MRS experiments two Kevlar 49 fibres were used as strain sensors. Moreover, these sensors were located in a pure resin region as seen in Figure 1b. For this reason the mechanical interactions with reinforcing chopped graphite fibres and the other sensor were neglected in the EIM computations. Effectively, the model used to extract the composite strain from the MRS experimental data was obtained from eqn (3-6) by putting inclusions volume fraction $v_f = 0$, neglecting the interactions between the sensors, and putting the Eshelby tensor for long fibres in place of the Eshelby tensor for spheres.

## 3 Experimental results

### 3.1 Materials tested

The unidirectional graphite/PMR-15 polyimide composites were manufactured at the NASA Glenn Research Centre in the form of 152 × 152 × 1 mm plates. Before curing, the Al inclusions were suspended in acetone and painted on top of the first unidirectional prepreg ply surface. After drying they were covered by the subsequent plies to form a laminate. The distributions of Al inclusions were determined using scanning electron microscopy. This work has been done at the University of Denver. The analysis showed that the average area fraction of Al inclusions in a cluster was 40% ± 7% and most of the inclusions were located 0.1 mm under the surface of the sample. A representative example of embedded Al inclusions is presented in Figure 1a. The following elastic properties of polyimide resin and Al inclusions were used in the numerical computations: $E^M$=4.5 GPa, $\nu^M$=0.36 and $E^I$=71 GPa and $\nu^I$=0.35, respectively (Benedikt et al. [1]).

The chopped graphite fibre/epoxy matrix composite samples with embedded Kevlar-49 fibres were fabricated at the LANL Engineering Sciences and Applications Division facilities. The composite samples were manufactured in the following way. First, two Kevlar-49 fibres were firmly attached to a mould; the fibres were positioned perpendicular to each other. Second, the mould was

filled with uncured epoxy containing chopped graphite fibres. The resin was allowed to cure before the sample was taken out from the mould. Two Kevlar-49 fibres oriented along the sample longitudinal and transverse directions are shown in Figure 1b. The following elastic properties of epoxy resin and Kevlar-49 fibres were used in the computations: $E^M$=4 GPa, $\nu^M$=0.36 and $E^I$=124 GPa and $\nu^I$=0.3, respectively. The thickness of the composite sample was 2.4 mm and Kevlar fibres were located 0.3 mm under the surface of the sample. The samples were manufactured in a form of rectangular plates.

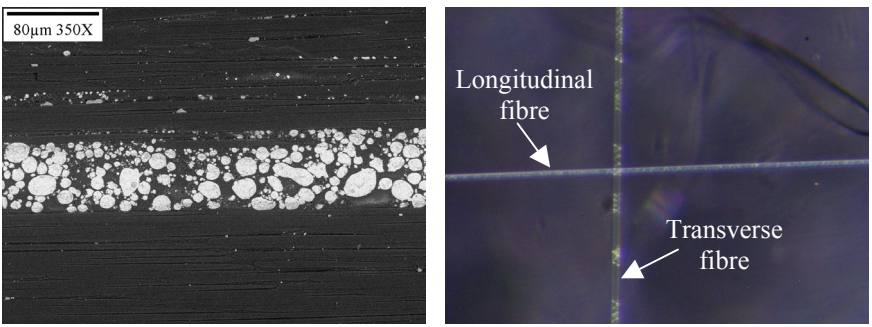


Figure 1: Examples of embedded (a) Al inclusions (Benedikt et al. [1]) and (b) Kevlar 49 fibres.

### 3.2 Four-point bending tests

The bending moment applied to the composite plates was generated by a four point bending fixture. The magnitude of the prescribed bending was controlled by a displacement of fixture's outer pins monitored by a micrometer. After the desired value of the strain was applied, the specimen was irradiated with either X-ray or laser beam and the strains inside the sensors corresponding to a given pins displacement were obtained.

Longitudinal strains measured in two Kevlar-49 fibres oriented along the sample longitudinal and transverse directions are presented in Figure 2. The MRS measurements were done as a function of the displacement of fixture outer pins. Three different measurements were taken from random locations on the fibres for each value of the pins displacement to evaluate the experimental scatter. In Figure 2 we show the average strains and respective standard deviations of the experimental data. The fibre strains for the displacement smaller than 2 mm are not shown in Figure 2, since the accuracy of these measurements was affected by the sliding of the pins on the sample surface and compressive residual strains in fibres. It is seen in the shown figure that there is a linear relationship between measured strains and the magnitude of the bending. It was determined using the least square method that the slope of the fibre strain vs. pins displacement was 13,910 ± 320 με and -550 ± 200 με per 1 mm displacement for longitudinal and transverse fibre, respectively. These values were subsequently used to determine the internal strains in chopped fibre composites caused by bending.

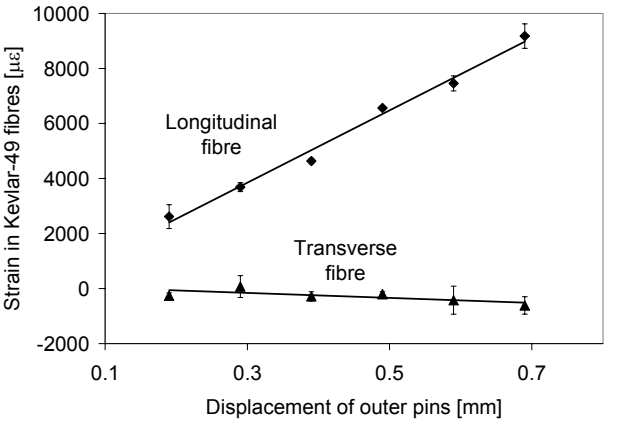


Figure 2: MRS strains in two Kevlar-49 fibres as a function of pins displacement.

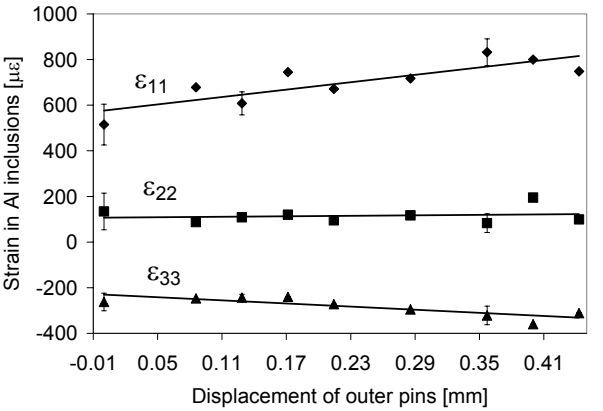


Figure 3: XRD strains in the Al inclusions as a function of pins displacement (Benedikt [1]).

Strains in the Al inclusions embedded in the unidirectional composite as a function of external bending are shown in Figure 3. The data presented in this figure was taken from Benedikt et al. [1]; the XRD experiments were done at the University of Denver. For pins displacements of 0, 0.13, and 0.36 mm three separate XRD strain measurements were done to evaluate the experimental scatter. The shown error bars represent the standard deviation of the experimental data. For the remaining values of pins displacements one strain measurement per given displacement value was made. All three principal strain components measured in the embedded inclusions were linearly changing as a function of the applied bending. However, it was discovered that for large

bending displacements (more than 0.5 mm) embedded Al inclusions yield plastically (Benedikt et al. [4]). The plastic effects in Al inclusions are not discussed in this work. Based on the experimental data shown in Figure 3, it was also determined that the $\varepsilon_{11}^{\text{X-Ray}}$, $\varepsilon_{22}^{\text{X-Ray}}$, and $\varepsilon_{33}^{\text{X-Ray}}$ strains changed by 540 ± 80 με, 40 ± 50 με and -230 ± 35 με per 1 mm displacement, respectively. It should be noted that the reported uncertainties for the XRD experiments are significantly smaller than the corresponding errors for MRS experiments.

## 4 Numerical results: composite strains as a function of prescribed bending

Model presented in section 2.3 was used to extract composite strains generated by four-point bending. For unidirectional polyimide matrix composites with embedded Al inclusions 100 clusters consisting of N=60 inclusions each were randomly generated. The volume fraction of the inclusions in each cluster was $v_f$=40%. The uncertainty of $\varepsilon^{\text{X-Ray}}$ was determined in section 3.2. Ten different values of strains $\varepsilon^{\text{X-Ray}} \pm \Delta\varepsilon^{\text{X-Ray}}$ corresponding to 1 mm displacement were randomly generated for each cluster. Altogether, 1000 cases of different clusters and $\varepsilon^{\text{X-Ray}} \pm \Delta\varepsilon^{\text{X-Ra}}$ strains were used in the computations to extract the average composite strains and their respective uncertainties. The results of these computations are presented in Table 1. For MRS measurements in Kevlar-49 fibres the numerical model used to extract the composite strains was much easier to implement numerically. No interactions between sensors were considered in the numerical model. Similarly as in the case of Al inclusions, the uncertainty $\Delta\varepsilon^{\text{MRS}}$ was assumed to be the same as the error of the MRS experimental data (Figure 2). Composite strains extracted from the measurements in Kevlar-49 fibres are presented in Table 1.

Table 1: Strains in unidirectional and chopped fibre composites per 1mm of outer pins displacement.

| | $\varepsilon_{11}$ [με] | $\varepsilon_{22}$ [με] | $\varepsilon_{33}$ [με] |
|---|---|---|---|
| Unidirectional fibre composite (sensor: Al inclusions, XRD) | | | |
| Lévy solution | 6570 | -1440 | --- |
| XRD and EIM | 6050 ± 900 | 560 ± 560 | -2290 ± 380 |
| XRD and EIM (no interactions) | 6100 ± 920 | 551 ± 563 | -2370 ± 385 |
| Chopped fibre composite (sensor: Kevlar 49, MRS) | | | |
| Lévy solution | 13200 | -2820 | --- |
| MRS and EIM | 13910 ± 320 | -550 ± 200 | --- |

To validate the EIM approach, the internal strains in a composite generated by four-point bending were computed using an approximate Lévy solution (Reddy [8]). Five terms of Fourier series were used in the numerical computations. In Table 1 composite strains at locations occupied by the sensors

computed using the Lévy procedure are compared with the strains determined from the embedded sensors. It can be concluded that $\varepsilon_{11}$ strain computed using the Lévy solution and the embedded sensors approach agreed reasonably well for both composite architectures. The discrepancy between the analytical predictions and experimental data for $\varepsilon_{22}$ was caused by the fact that the bending for the analytical model was generated by prescribing constant line load to a sample. As a result, a saddle-like region was formed between two inner pins. In reality, the creation of the saddle region was suppressed presumably by the friction between the pins and the sample, which resulted in measured $\varepsilon_{22}$ strains having smaller magnitude than indicated by the analytical model. The through-thickness strain $\varepsilon_{33}$ was not computed using the Lévy method.

In section 3.2, the standard deviations of $\varepsilon_{11}^{MRS}$ and $\varepsilon_{11}^{X\text{-}Ray}$ measured in Kevlar-49 and Al sensors were estimated (320 με and 80 με for Kevlar-49 and Al inclusions, respectively). Based on these estimates, we conclude that the XRD strains in the Al inclusions were four times more accurate than the MRS strains in Kevlar-49 fibres. However, according to the data presented in Table 1 the longitudinal and transverse strains in composites were actually more precisely determined using MRS. The standard deviations of $\varepsilon_{11}$ in a composite due to 1 mm pins displacement are 320 με and 900 με for MRS and XRD tests, respectively. MRS yielded better estimates of the composite strain $\varepsilon_{11}$, since the longitudinal strain transfer to a fibre-sensor was significantly larger than the strain transfer to Al inclusions. It was also found that the longitudinal strain transfer to a fibre was virtually not affected by the elastic properties of the sensors. In addition, the longitudinal strain in a fibre was almost identical to the corresponding composite strain. This is a consequence of the fact that $S_{11jj}$ (j=2 or 3) components of the Eshelby tensor for a fibre are zero, where $x_1$ is the fibre direction. On the other hand, it can be shown using eqn (3-6) that the strain transfer to spherical inclusions depends on elastic properties of the matrix and inclusions. Therefore, if spherical sensors are used, the properties of the matrix and inclusions have to be known to extract composite strains. In addition, it is shown in Table 1 that the interactions between the Al inclusions had only a minor effect on the computed composite strains. Moreover, spherical inclusions could be used to determine all three principal strains in a composite. Fibre sensors can be only used to determine longitudinal strains. Therefore, two perpendicular fibres had to be used to determine $\varepsilon_{11}$ and $\varepsilon_{22}$.

## 5 Conclusions

- XRD and MRS can be used to determine strains generated by a four-point bending fixture in investigated polymer matrix composites
- Composite strains were more accurately determined using long fibres as sensors; spherical inclusions yielded less accurate results
- All three principal strains in a composite were determined using spherical inclusions; long fibres can be used to determine composite strains only along their longitudinal direction

- The average interactions between the Al inclusions can be neglected in the computations leading to the extraction of composites strains

## Acknowledgements

This research was performed at the Los Alamos National Laboratory, operated by the University of California for the Department of Energy (W-7405-ENG-36). The authors wish to thank Dr. M Kumosa and Mr. J Charles.

## References

[1] Benedikt B, Predecki P, Kumosa L, Armentrout D, Sutter JK, Kumosa M, The use of X-ray diffraction measurements to determine the effect of bending loads on internal stresses in aluminium inclusions embedded in a unidirectional graphite fibre/PMR-15 composite, *Composite Science and Technology*, vol. 61, p 1995-2006, 2001.

[2] Predecki P, Barrett C, Stress Measurement in Graphite/Epoxy Composites by X-Ray Diffraction from Fillers. *J. Comp. Mat.*, vol. 13, p 61-71, 1979.

[3] Galiotis C, Interfacial Studies on Model Composites by Laser Raman Spectroscopy. *Composite Science and Technology*, vol. 42, p 125-150, 1991.

[4] Benedikt B, Kumosa M, Predecki P, An Evaluation of Residual Stresses in Graphite/PMR-15 Composites by X-Ray Diffraction. *Acta Mat.*, in press.

[5] Noyan IC, Cohen JB, Residual Stress. Measurement by Diffraction and Interpretation. Springer-Verlag, New York, 1987.

[6] Benedikt B, Lewis M, Rangaswamy P, Multi-Inclusion Model for Particulate Composites with Periodically and Randomly Distributed Reinforcements. *Journal of the Mechanics and Physics of Solids*, submitted.

[7] Eshelby JD, The Determination of the Elastic Field of an Ellipsoidal inclusion, and Related Problems. *Proc. R. Soc. London*, vol. A241, p. 376-396, 1957.

[8] Reddy JN, Mechanics of Laminated Composite Plates. Theory and Analyses. CRC Press, 1997.